# BOLOMETER FOR MEASUREMENTS ON HIGH-TEMPERATURE PLASMAS

J. Schivell, G. Renda, J. Lowrance, and H. Hsuan

Plasma Physics Laboratory, Princeton University

Princeton, New Jersey 08544

PPPL--1910

DE82 018629

ABSTRACT

A bolometer has been developed, based on a thin, die-cut platinum grid. It can survive high temperatures and the neutron and gamma radiation expected in the Toroidal Fusion Test Reactor (TFTR). The platinum resistance is measured with a square-wave carrier system to minimize sensitivity to ambient electromagnetic interference. Electrical power fed back to the sensor holds its temperature constant and provides an output directly proportional to absorbed radiation power. With a bandwidth of 50 Hz the noise is equivalent to 100 $\mu W/cm^2$. Methods are described for dealing with the background effects expected to contribute to bolometer heating.

## INTRODUCTION

The purpose of using bolometers in fusion research is to measure the plasma total radiated power.[1,2] This measurement complements spectroscopy, which is sensitive to specific lines or portions of the spectrum. Since a bolometer responds to any energy which it absorbs, it is sensitive to electromagnetic radiation, neutral atoms, and charged particles from a plasma. With an uncollimated bolometer we assume that the power it receives is representative of the total power reaching the wall of the vessel, by whatever means. However, with a collimated bolometer we usually assume that the contribution of neutral atoms is negligible and that charged particles cannot reach the detector. Hence, in this case we have a measurement of electromagnetic radiation from the plasma integrated along a chord. With a set of chords fanning across a plasma column, we integrate over the column to obtain the total radiated power, and we perform an Abel inversion[3] to obtain the intensity of radiation as a function of radius. This distribution can reveal the type[4] and amount[5] of impurities present in a plasma. For quasi-steady-state discharges with electron temperatures in the keV range, the location of the radiation sources corresponds approximately to the species radiating -- heavy elements in the center, medium at intermediate radii, and light elements, including neutral hydrogen, near the outside.[6]

On the Princeton Large Torus (PLT) and the Poloidal Divertor Experiment (PDX) we use detectors made with metal-oxide thermistors, but they will not tolerate the nuclear radiation and high temperatures expected on the Toroidal Fusion Test Reactor (TFTR). For TFTR we have developed a new type of bolometer, based on a thin platinum grid and a resistance measurement circuit using square-wave excitation and synchronous detection.

## DESIGN OF BOLOMETER

### Currently Used System

In the usual type of bolometer used on PLT and PDX, the thermistor[7] is mounted on the back face of a 38 μm copper foil (Fig. 1). Epoxy is used both to insulate the thermistor from the copper and to hold it in place. The foil is mounted on a stainless steel tube, which, in turn, is mounted on a copper heat sink. A reference thermistor is mounted on the heat sink. The thermistor is 0.5 mm square and 38 μm thick, with a nominal resistance of 25 kΩ.

The changing resistance is measured by Wheatstone bridge circuit. Between plasma discharges a control circuit automatically keeps the bridge in balance; when triggered, just before a discharge, it holds the balancing currents at fixed values for several seconds so that the imbalance due to absorbed power can be detected. Separately, the time response curve of each bolometer is obtained by flashing a photographer's strobe (flash duration, about 1 ms) at it and recording the output. This curve is used in unfolding the absorbed power from measured temperature-versus-time data.

### Operating Environment on TFTR

The neutron dose at the bolometers over the lifetime of the machine is expected to be $2 \times 10^{17}$ neutrons/cm$^2$, and the total dose, including gammas, to be $1 \times 10^8$ rad (Si). Since the bolometers will be attached to the machine vacuum vessel, they will experience temperatures during bake-out as high as 200°C. Furthermore, since the vacuum vessel will get quite hot during operation, the bolometers will have to operate without loss of accuracy from 15°C to 100°C. In addition, they are required to have minimal outgassing in a vacuum of $10^{-8}$ Torr.

Sensor Choice

The thermistors which we use currently have a maximum temperature limitation of 150°C,[7] and the resistance is a strongly nonlinear function of temperature. We tested a thermistor bolometer in a fission reactor; after 45 minutes at 5 x $10^3$ rad/s (total dose 1.4 x $10^7$ rad) the room-temperature resistance had changed by 40%. The change was most likely due either to the absorbed dose or to effects of the temperature during irradiation. Furthermore, there was a three-fold increase in noise during irradiation.

A number of other types of sensors were considered. Pyroelectric detectors were thought to be too sensitive to nuclear radiation, as would be the necessarily adjacent preamplifier. Thermopiles might also be subject to radiation-induced noise at the junctions, but in any case do not have the possibility of ac operation. We also considered using a radiation absorbing diaphragm, the deflection of which would be sensed by either a capacitance change, a shift in a microwave cavity, or an interferometer. However, the complications of a mechanical system did not seem to be offset by significant advantages. Finally, there is the method of a radiation-absorbing foil, the temperature of which is monitored by an infrared detector. This method was rejected because the sensitivity is marginal for this application and because the optics are a significant complication.

The sensor chosen for use in the new bolometers is a commercially available die-cut platinum grid which is sold as a strain gage or a temperature sensor.[8] The fact that the thickness, 3.5 μm, is one-tenth that of the thermistors offsets the ten times smaller resistance-temperature coefficient of platinum, compared with the thermistors. Platinum has a well-known resistance-temperature coefficient, constant to within 2% over the range

0 to 100°C, which simplifies operation at high ambient temperature. After reactor irradiation to 5 x $10^7$ rad, the resistance-temperature coefficient of platinum grid samples was unchanged, as expected. There was no increase in noise during irradiation.

A further advantage of the commercially available platinum sensor is that the thickness of 3.5 μm is sufficient to stop energetic X rays from the plasma. The absorption length of platinum is 3.5 μm for X rays of 9 keV energy. The amount of radiation above 9 keV is expected to be quite small. For extreme plasma temperatures we will probably need to check the detector transmission loss by using a thicker detector.

## Detector Design

The sensor is mounted over a trough in an anodized aluminum heat sink and cemented in place with epoxy or polyimide at the ends of the strands (Fig. 2). An identical reference sensor is cemented to the solid back face of the heat sink so that the strands are in good thermal contact with the sink over their entire length. If rapid thermal drift were a problem, the reference sensor could be cemented to an area on the front face of the sink, not over the trough.

## Resistance Measurement and Control Circuit

The active and the reference sensors and two fixed resistors at the electronics chassis are connected to form a Wheatstone bridge. To reject pick-up voltages induced by the changing electromagnetic fields of the tokamak and by the neutral beams, we excite the bridge with a square wave at 20 kHz. To eliminate the need for a reactance adjustment the synchronous detector is gated off for a time after each reversal of the square wave.

A feedback circuit has been designed that allows the sensor to be maintained at constant temperature by modulating the electrical power dissipated in the sensor. This provides a way to measure directly the power absorbed from the plasma. In this mode there is an output proportional to absorbed power, and the result is independent of the sensor thermal capacitance and thermal resistance over a reasonable range of variation of these parameters. Thus, calibration and data analysis are simplified considerably. The behavior of the constant temperature feedback system is analyzed in the Appendix. Alternatively, this circuit can be operated in the conventional temperature measuring mode. To determine the absorbed power versus time in this mode, it is necessary to unfold a detector cooling curve from the measured sensor temperature versus time.

Another feature of the circuit is a built-in electrical power pulse to calibrate the detector. A dc offset is added to the square wave applied to the bridge; the self-heating power to all four arms of the bridge is increased, but the two fixed resistors have a negligible temperature coefficient, and the reference sensor is held at practically constant temperature by the heat sink. Thus, there is a change in the active sensor only. This electrical calibration can be used in either the open-loop (temperature) mode or the closed-loop (power) mode.

## Magnetic Field Interaction

There is a problem in using this kind of bolometer system in a strong magnetic field -- the alternating $\vec{I} \times \vec{B}$ force on the strands of the sensor grid can excite vibrations. The strain-gage effect produces noise in the output signal. Tests have shown a sharp onset of this noise at about 400 gauss for the usual sensor current of 5 mA. We have been testing several

special versions of the sensor which reduces this effect. In one version the grid is cemented to a backing of 7.5 μm kapton and 3.5 μm platinum, and in another the grid is made of two layers of platinum (with kapton between), arranged so that opposite currents in the layers of each strand produce cancelling forces. So far we have found that the backed version is unaffected by transverse magnetic field up to 10-15 kG. In TFTR we plan to orient the strands parallel to the toroidal field, so that the transverse field is well below 10 kG.

## DATA ANALYSIS

When the system is used with the temperature feedback loop open, the thermal characteristics of the detector must be used in the data analysis. The detector is used in vacuum, and cooling by radiation is negligible. Therefore, the cooling is analyzed as a one-dimensional conduction problem in rectangular coordinates. Any strand behaves as though it were a part of an infinite slab, since all heat flow is toward the ends of the strands, which would correspond to the faces of the slab. First we consider the strands absorbing a quantity, $\Delta\mathcal{E}_A$, of energy per unit area in a negligibly short time. Let the thermal capacity of the sensor per unit area be $S = \rho C\varepsilon$, where $\rho$ is density, $C$ is specific heat, and $\varepsilon$ is thickness. For a laminated sensor, like the kapton-backed platinum grid, $S$ is the sum of $\rho C\varepsilon$ for both layers. The temperature rise is $\Delta T = \Delta\mathcal{E}_A/S$. As the sensor cools, the resistance is proportional to the average temperature over the strand. At time $t = 0$ the average is $\bar{T}_\delta(0) = \Delta T$, and for all later times it is given by[9]

$$\bar{T}_\delta(t) = 0.811\, \bar{T}_\delta(0) \sum_{n=0}^{\infty} \frac{1}{(2n+1)^2}\, e^{-(2n+1)^2\, t/\tau}, \qquad (1)$$

where $\tau = 4\ell^2/\pi^2 D$, $2\ell$ is the strand length, and D = the thermal diffusion coefficient. For an arbitrary input of power per unit area, $P_A$, as a function of time, we have

$$\bar{T}(t) = \int_0^t dt' \, P_A(t') \, \bar{T}_\delta (t - t') \quad . \tag{2}$$

For a constant power input, $P_{Ac}$ starting at t = o, we obtain

$$\bar{T}_c(t) = 0.811 \frac{P_{Ac}\tau}{S} \sum_{n=o}^{\infty} \frac{1}{(2n+1)^4} \left[1 - e^{-(2n+1)^2 \, t/\tau}\right] \quad . \tag{3}$$

To measure $\tau$ experimentally, we apply a long electrical power pulse and record the temperature versus time. Eq. (3) is fitted to the data to obtain $\tau$. The steady-state temperature rise, $\bar{T}_c(\infty)$, gives the thermal resistance, $R_{th}$, by $R_{th} = \bar{T}_c(\infty)/P_{Ac}A$, where A is the sensor area. Letting $t \to \infty$ in Eq. (3), we get $\bar{T}_c(\infty) = 0.823 \, P_{Ac}\tau/S$. Therefore, $R_{th} = 0.823 \, \tau/C_{th}$, where the thermal capacity is $C_{th} = AS$. Finally, we have the somewhat unusual relationship $R_{th} \, C_{th} = 0.823 \, \tau$.

A discrete version of Eq. (2) is used in unfolding the data from a plasma discharge. The data $\bar{T}_i$ are taken at times $t_i$, and we let

$$\bar{T}_i = \sum_{j=1}^{i-1} \Delta t \, R_{ij} \, P_{Aj} \quad , \text{ for } i = 2,N \tag{4}$$

where $\bar{T}_\delta(t-t') \rightarrow R_{ij}$. The value of $R_{ij}$ depends only on i-j. $\bar{T}_1 = 0$, and $\bar{T}_2 = \Delta t\ R_{21}\ P_{A1}$, which is solved for $P_{A1}$. Then, for the values of $P_A$ at all other times, we rearrange Eq. (4):

$$P_{Ai} = \frac{1}{\Delta t\ R_{(i+1)i}} \left[\bar{T}_{i+1} - \sum_{j=1}^{i-1} \Delta t\ R_{(i+1)j}\ P_{Aj}\right], \quad \text{for } i = 2, N-1 . \qquad (5)$$

TESTS ON EXISTING TOKAMAKS (Fig. 3)

The platinum sensor and the measurement and control circuit have been used on PLT and PDX for several months, looking at the same region of the plasma as other bolometers. The solid angle viewed is 2.8 millisteradian. The performance with and without the temperature feedback loop closed has been evaluated. Noise levels, in terms of equivalent energy flux at the detector, are given in Table 1. As expected, the noise value comes out to be the same whether the power is determined from the open loop temperature signal or directly from the closed loop power signal. These noise levels are as low or lower than those for our thermistor bolometers.

On TFTR a typical solid angle for a bolometer will be 10 msr. With a 1 MW plasma we expect to see power at the detector of the order of 2 $mW/cm^2$. A 10 ms averaging time will make the noise less than 5% of this signal. For a 30 MW plasma we may be able to use 1 ms or finer resolution. The noise-bandwidth relationship is calculated in the Appendix.

## ADDITIONAL CONSIDERATIONS

### Blackening

The majority of radiation is expected to be in the far UV and soft X ray.[4] However, it would be very desirable to blacken the platinum sensors for two reasons: 1) Platinum reflects some of the incident light, even in the vacuum UV. As seen in Fig. 4, the reflectance hovers around 15% down to 400Å. 2) An absorption coefficient which was flat from the visible or near UV through the vacuum UV would simplify calibration considerably, since ordinary light sources could be used. We are currently testing three approaches: blackening by electrodeposition from a solution of platinum chloride, blackening with acetylene soot, and using the kapton backing as the absorbing face.

### Separation of the Contributions to Bolometer Heating

The bolometers will, of course, respond to any absorbed energy. In addition to the electromagnetic radiation from visible through X ray, for which this diagnostic instrument is intended, there will be "background" inputs, which not only are errors in the measurement of impurity radiation but are in themselves not likely to be measurable by these bolometers in a meaningful way. These background energy inputs are synchrotron radiation, infrared radiation from the hot inner "bumper" limiters (continuous around the torus), neutron and gamma radiation, and neutral atoms. On TFTR the synchrotron radiation from hot, dense plasmas[10] can be as large as the impurity radiation. Since synchrotron radiation is strongly reflected by the walls, it is very difficult to correct for it by using results of other measurements. Unless one can calibrate the absorption of the detector at

synchrotron wavelengths, one must block out the synchrotron radiation with a fine mesh (e.g., 50 μm spacing). Under the worst conditions,[11] the infrared may also be nearly as large as the impurity radiation. This contribution we plan to subtract, making use of measurements by an infrared TV camera. During D-T shots the heating of the platinum grid by neutrons and gammas is expected to be of the same order as impurity radiation.[12] Since the heating of the sensor by $\underline{n}$ and $\gamma$ radiation depends on the location, the spectrum, and the sensor material, it is not practical to calculate the heating from other measurements of $\underline{n}$, $\gamma$ flux. Instead, it is planned to have a covered bolometer, which will be heated only by $\underline{n}$,$\gamma$ flux, next to each regular bolometer. The signal from the covered detector will be subtracted from the regular signal. Finally, the flux of neutrals is strongly dependent on location.[13] The current plan is to use the bolometer primarily at locations where the neutral flux is small.

TABLE 1

NOISE AS A FUNCTION OF AVERAGING TIME

(measured rms $mW/cm^2$ at the detector)

| Averaging time: | 1 ms | 10 ms | 30 ms |
|---|---|---|---|
| Open loop | 3 | 0.1 | 0.02 |
| Closed loop | | .09 | |

ACKNOWLEDGMENTS

We would like to thank K. Young for his continuing support and encouragement of this work, D. Rorer for his assistance in testing at a fission reactor at Brookhaven National Laboratory, and V. Mastrocola for his effort in fabrication and testing of the system. We are also grateful to the people at Dentronics, Inc., for their helpfulness in fabricating modified sensors. This work was supported under U.S. DOE Contract Number DE-AC02-76-CHO-3073.

## APPENDIX

## BOLOMETER ELECTRONICS

A system block diagram of the bolometer electronics is shown in Fig. 5. The major subdivisions consist of a Wheatstone bridge circuit containing the platinum sensor and similar reference resistor, a square wave modulator, double correlated integrator, synchronous demodulator, and an auto-balance circuit. To facilitate calibration, the system also provides the capability of applying electrical power pulses to the sensor to measure its thermal properties and a fixed electrical resistance change to calibrate the system gain (volts/°C).

Through a user command, the bolometer system is configured in one of two modes (temperature or power). In the temperature mode, the output voltage is proportional to the temperature change of the sensor due to the absorbed radiation. Depending on the type of platinum foil sensor being used, thermal time constants range from 30 ms to several tenths of a second. In the power mode the output voltage is directly proportional to the absorbed radiation power. Since it is a closed loop system, the designer can control the loop temporal characteristics. In the temperature mode, the time response is totally dependent on the sensor.

If the thermal characteristics are not accurately known, differentiation of the temperature data will produce large power magnitude errors and temporal distortion. In the power mode, the power magnitude is insensitive to the thermal resistance, and the closed loop bandwidth is inversely proportional to the thermal capacitance. Although system bandwidth can be controlled by the loop gain, one cannot make an arbitrary choice in loop bandwidth. The noise is proportional to $f^{3/2}$. The same noise-bandwidth relationship also applies in the temperature mode after the data has been converted to power through unfolding by the computer.

## CONSTANT TEMPERATURE CONTROL SYSTEM MODEL

Figure 6 depicts the model used for the analysis. The exact solution of the thermal characteristics of the sensor takes the form of a series of exponential terms [Eq. (3), main text]; however, a lumped thermal RC is used in this analysis. This has proved sufficiently accurate to model the feedback loop behavior.

As can be seen from the model, prior to t(0), a reference power is applied through a summing junction, establishing an equilibrium temperature for the sensor. The temperature is measured by $G_T$, and its output voltage is applied to $G_{V1}$. The signal from $G_{V1}$ is connected to a summing junction and a sample and hold circuit whose output is applied to the same summing junction but with the opposite polarity. The net effect is to produce a zero input to $G_{V2}$ prior to t(0). Additionally, the junction has a temperature offset input which is adjusted to produce the same level of power in the sensor that was established by the power reference input. A trigger at t(-0) causes the power loop to be closed; normally 30 ms is allowed for the loop to reach equilibrium.

The loop parameters (see Fig. 6) and typical values are:

$G_T$ = Voltage output per unit temperature change of sensor = $2.5 \times 10^{-3}$ V/°C.

$G_V$ = $G_{V1}\ G_{V2}$ = Voltage gain amplifier = $2 \times 10^{4}$.

$G_W$ = Sensor electrical power amplifer = $2 \times 10^{-3}$ W/V.

$G_L$ = $G_T\ G_V\ G_W$ = loop gain = 0.1 W/°C.

$R_T$ = Sensor thermal resistance = 800 °C/W.

$C_T$ = Sensor thermal capacitance = $1.2 \times 10^{-4}$ J/°C.

Using control system analysis techniques[15] the following equations can be written at t(0):

$$\frac{\Delta P_o(s)}{P_i(s)} = -\frac{1}{\beta + 1/A} = -\frac{1}{1 + G_L R_T/[SC_T R_T + 1]} \quad , \tag{A1}$$

$$\frac{\Delta P_o(s)}{P_i(s)} = -\frac{G_L}{C_T[S + 1/C_T R_T + G_L/C_T]} \quad . \tag{A2}$$

Applying a step function yields

$$\Delta P_o(s) = -\frac{P_i(s) G_L}{SC_T[S + 1/C_T R_T + G_L/C_T]} \quad . \tag{A3}$$

Taking the inverse Laplace transform

$$\Delta P_o(t) = -\left[P_i(t)\ G_L R_T/[G_L R_T + 1]\right]\left[1 - e^{-t[1/R_T C_T + G_L/C_T]}\right] \quad . \tag{A4}$$

For $G_L R_T >> 1$

$$\Delta P_o(t) \approx -P_i(t)\left[1 - e^{-tG_L/C_T}\right] \quad . \tag{A5}$$

The significance of Eq. (A5) is that $\Delta P_o$ is proportional to $P_i$ and the system time constant, $C_T/G_L$, can be controlled by the electronic gain of the loop. For the above parameters $C_T/G_L$ = 1.2 ms. For comparison, the sensor cooling time $R_T C_T$ = 96 ms.

The photographs of Fig. 7 show the bolometer's response to an input power pulse in both the temperature and power mode. In the power mode (closed loop), the gains were set to a calculated system time constant of 2.5 ms (63% of final value). Photographs (A) and (B) indicate that there is good agreement with Eq. (A5). The input power for (A) was an electrical pulse and the input power source for (B) was a quartz halogen lamp which was shutter controlled. Photograph (C) shows the bolometer's response in the temperature mode to the same magnitude of power that was applied in (A).

## CLOSED LOOP NOISE MODEL

The noise model is shown in Fig. 8. To analyze the noise behavior, the temperature offset, temperature reference, and input power nodes have been grounded. With these inputs grounded, we can move the $GV_1$ block to the right of the summing junction. The loop parameters and definitions are the same as described for the Constant Temperature Control System Model. Since the electrical resistance of the platinum sensor is approximately 50 ohms, the associated theoretical Johnson noise is less than 1 nV/ $\sqrt{\text{Hz}}$. This is less than the preamp noise and can be neglected. The transfer function $G_T$ is associated with the Wheatstone bridge and its quiescent power. Since the top of the bridge has a common node, noise sources which are introduced by the modulator are rejected by the common mode gain of the differential preamplifier. Therefore, the only significant components of noise are those which are introduced by the preamplifier as depicted by the $e_n$ generator shown in the noise model. With a carrier of 20 kHz the frequency of interest is between 19.5 kHz and 20.5 kHz. For this narrow spectrum, the magnitude of $e_n$ is a constant. The constant K is introduced which will modify the magnitude of $e_n$. This constant is explained later in the paper.

Using the model shown in Fig. 8, and Laplace notation, the following equations can be written:

$$\frac{P_n}{Ke_n} = -\frac{1}{\beta + 1/A} = -\frac{1}{G_T R_T/[SC_T R_T + 1] + 1/G_V G_W} \quad . \tag{A9}$$

For $\frac{G_T G_V G_W}{C_T} >> \frac{1}{C_T R_T}$

$$\frac{p_n}{Ke_n} = - \frac{G_V G_W [S + 1/C_T R_T]}{S + G_T G_V G_W / C_T} \quad . \tag{A10}$$

Converting to the frequency domain

$$p_n = - \frac{Ke_n G_V G_W [j\omega + 1/C_T R_T]}{j\omega + G_T G_V G_W / C_T} \quad . \tag{A11}$$

A spectral noise density plot of Eq. (A11) in arbitrary magnitude and frequency units is shown as curve (a) in Fig. 9.

To clarify the significance of this figure, two additional curves (b & c) are drawn. (When the parameter $G_T$ or $C_T$ is changed, a corresponding change is made to $G_L$ [Eq. (A4)] to maintain the same time response.) Curve (b) shows the effect of decreasing the thermal capacitance by 2. Since the dominant region is region 2 this will result in a noise decrease approaching 2:1. Curve (c) shows the effect of increasing $G_T$ by 2. Again the noise will decrease in the order of 2:1. It is interesting to note that if the thermal resistance ($R_T$) is increased by 2, the magnitude of the noise below $f_1$ will decrease by 2. However, $f_1$ break frequency will occur one octave earlier resulting in a response following that of curve (a). This indicates that the thermal resistance has negligible effect on the system noise.

Of interest is the total rms noise in a given band which is defined as:

$$p_{nT} = \left[ \int_{f_a}^{f_b} p_n^2 \, df \right]^{1/2} \quad . \tag{A12}$$

In the output we pass a band from $f_a = 0$ to $f_b < f_2$, with $f_b >> f_1$. To simplify the equation and make evident the dominant terms we can compute the rms contribution from each of the two regions.

For region 1 we approximate $p_{n1}$ by

$$p_{n1} = Ke_n / G_T R_T \quad .$$

Then
$$p_{n1} = \left[ \int_{o}^{f_1} [Ke_n / G_T R_T]^2 \, df \right]^{1/2} \quad , \tag{A13}$$

and
$$p_{n1} = \frac{Ke_n f_1^{1/2}}{G_T R_T} \quad . \tag{A14}$$

For region 2 we approximate $p_{n2}$ by

$$p_{n2} = \frac{2\pi \, Ke_n C_T f}{G_T} \quad .$$

Then
$$p_{n2} = \left[ \int_{f_1}^{f_b} \left[ \frac{2\pi \, Ke_n C_T f}{G_T} \right]^2 df \right]^{1/2} \quad , \tag{A15}$$

and $$P_{n2} = \frac{2\pi\ Ke_n C_T\ [f_b^3 - f_1^3]^{1/2}}{\sqrt{3}\ G_T} \quad . \tag{A16}$$

In our case $f_b >> f_1$ and $P_{n1} << P_{n2}$

$$\therefore P_{nT} \approx P_{n2} \approx \frac{2\pi\ Ke_n C_T f_b^{3/2}}{\sqrt{3}\ G_T} \quad . \tag{A17}$$

Although this system utilizes a carrier, the magnitude of $e_n$ can be referred back to the input as one would in a dc system provided an appropriate scaling factor is used. This scale change comes about through the synchronous demodulator. The white noise can be broken down into a series of sinewaves, therefore, the only information required is the transfer function of the demodulator for non-synchronous sinewave inputs near the carrier frequency. It can be shown that, if the integration time is much less than than the total carrier period, the noise gain/signal gain = 2. If the integration time approaches the carrier period, the noise gain/signal gain = $4/\pi$. Because of other system constraints, the demodulator has a small integration time compared to the carrier period, resulting in a scale factor approaching 2. This should not be interpreted as meaning that the carrier system is 2:1 worse than a dc system. For a given quiescent power in the sensor, the signal amplitude across the bridge is I x $\Delta$R for a dc system, and for a symmetrical square wave, the amplitude for the same power is $I_{pk-pk}$ x $\Delta$R, resulting in twice the signal amplitude. Since the noise component frequencies are on both sides of the carrier, we have, in effect, twice the noise bandwidth. This will increase the rms noise by the $\sqrt{2}$. So the final scaling factor K $= 2\sqrt{2}$.

Using Eq. (A17) and introducing the above factor we have

$$P_{nT} \approx \frac{10\, e_n\, C_T\, f_b^{3/2}}{G_T} \quad . \tag{A18}$$

Measuring $e_n$ directly, $e_n$ = 12 nV/ $\sqrt{\text{Hz}}$ . Taking $f_b$ = 50 Hz leads to $P_{nT}$ = 2μW. The measured $P_{nT}$ is 2.4 μW, which is in reasonable agreement.

## REFERENCES


1. Examples of early uses of bolometers in fusion plasma research are those mentioned in H.J. Karr, E.A. Knapp, and J.E. Osher, Physics of Fluids 4, 424 (1961), and V.A. Burtsev, A.M. Stolov, and V.V. Shakhov, Sov. Phys.-Tech. Phys. 5, 1340 (1961).

2. H. Hsuan, K. Bol, R.A. Ellis, Nuclear Fusion 15, 657 (1975).

3. K. Bockasten, J. Opt. Soc. Am. 51, 943 (1961).

4. E. Hinnov, Princeton University Plasma Physics Laboratory report MATT-777 (1970).

5. R.V. Jensen, D.E. Post, W.H. Grasberger, C.B. Tarter, W.A. Lokke, Nuclear Fusion 17, 1187 (1977).

6. H. Hsuan, et al., Proc. Joint Varenna and Grenoble Int. Symp. on Heating in Toroidal Plasmas, Grenoble (1978).

7. Victory Engineering Corp., Springfield, N.J., "Thinistor," e.g., Model 43K1A500.

8. Dentronics, Inc., 60 Oak Street, Hackensack, N.J. Platinum temperature sensor type 902.

9. H.S. Carslaw, and J.C. Jaeger, Conduction of Heat in Solids, 2nd edition, (Oxford University Press, 1959), p. 97.

10. F. Pohl, Max-Planck-Institut fuer Plasmaphysik Report IPP 6/161 (1977).

11. R. Budny, 4th International Conference on Plasma-Surface Interactions in Controlled Fusion Devices, Garmisch-Partenkirchen, Federal Republic of Germany, April, 1980, and R. Budny, and C. Ludescher, 11th Symposium on Fusion Technology, Oxford, Sept., 1980.

12. L.-P. Ku, Princeton University Plasma Physics Laboratory Report PPPL-1711 (1980).

13. E.S. Marmar, Journal of Nuclear Materials, 76 & 77, 59-67 (1978).

14. J. Samson, Techniques of Vacuum Ultraviolet Spectroscopy, (John Wiley and Sons, Inc., 1967), p. 37.

15. C.J. Savant, Control System Design, 2nd Edition, (McGraw-Hill, 1964), pp. 1-30.

## FIGURE CAPTIONS

Fig. 1 Thermistor bolometer. Thermistor size is 0.5 x 0.5 x 0.04 mm. Copper foil thickness is 0.04 mm.

Fig. 2 Platinum grid bolometer, showing sensing grid mounted over ditch in heat sink, and reference sensor on the back. Heat sink is anodized aluminum.

Fig. 3 Line integrals of power radiated along a diameter of PLT: (a) bolometer signal (top curve) and unfolded power vs. time (bottom curve), (b) measured directly in the closed-loop mode. Response times for both smoothed to 10 ms. Conditions: (a) Ohmic-heating phase, plasma current 450 kA, voltage 1.2 V, density $1.6 \times 10^{13}$ $cm^{-3}$, four neutral beams injected from 450 to 600 ms, total beam power 2.6 MW, (b) at 400 ms current 380 kA, voltage 1.2 V, density $0.6 \times 10^{13}$ $cm^{-3}$.

Fig. 4 Normal incidence reflectance of platinum as a function of wavelength. (Ref. 14).

Fig. 5 Block diagram of bolometer electronics.

Fig. 6. Block diagram of constant temperature control system.

Fig. 7 Bolometer response to an input power pulse. (a) Response to electrical calibration pulse (power mode). (b) Response to shutter

controlled halogen lamp pulse (power mode). (c) Response to electrical calibration pulse (temperature mode).

Fig. 8 Block diagram of closed loop noise model.

Fig. 9 Power noise spectrum vs. frequency. (a) Spectral noise density plot of Eq. (A11) in arbitrary magnitude and frequency units. (b) Effect of decreasing the thermal capacitance by 2:1. (c) Effect of increasing $G_T$ by 2:1.

#81X1270

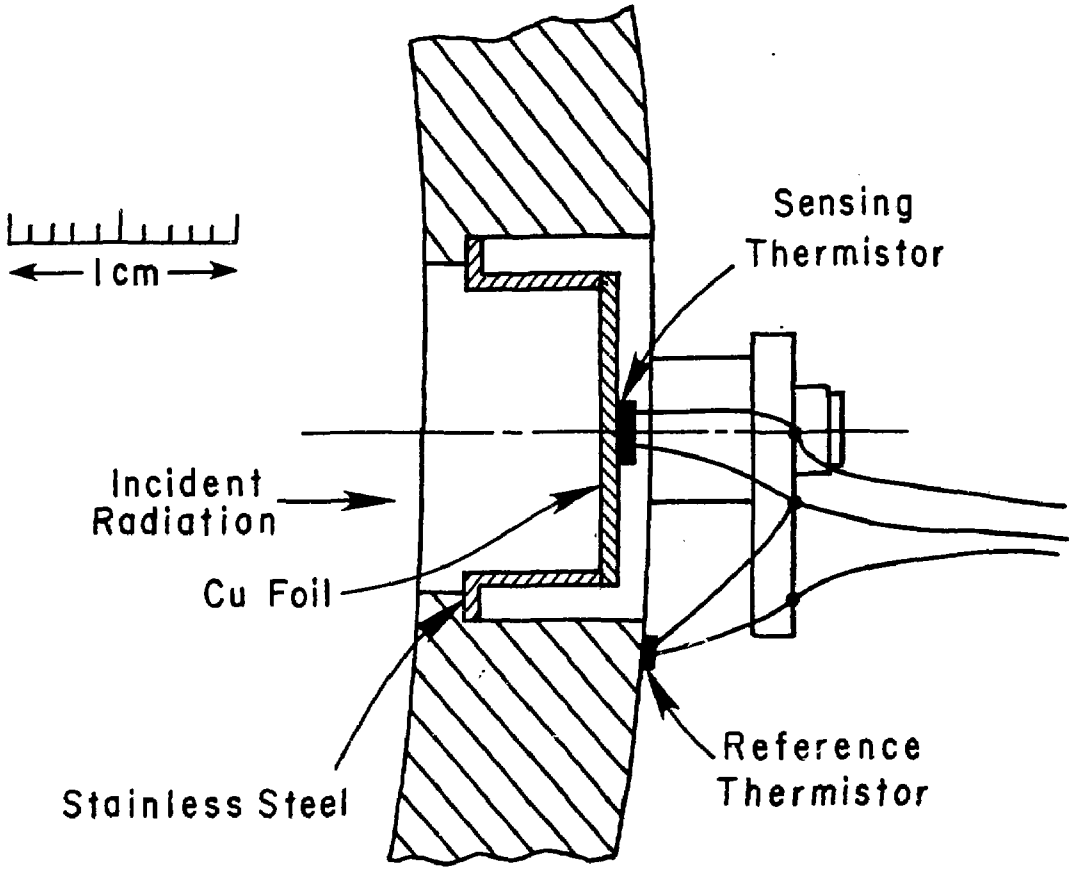


Fig. 1

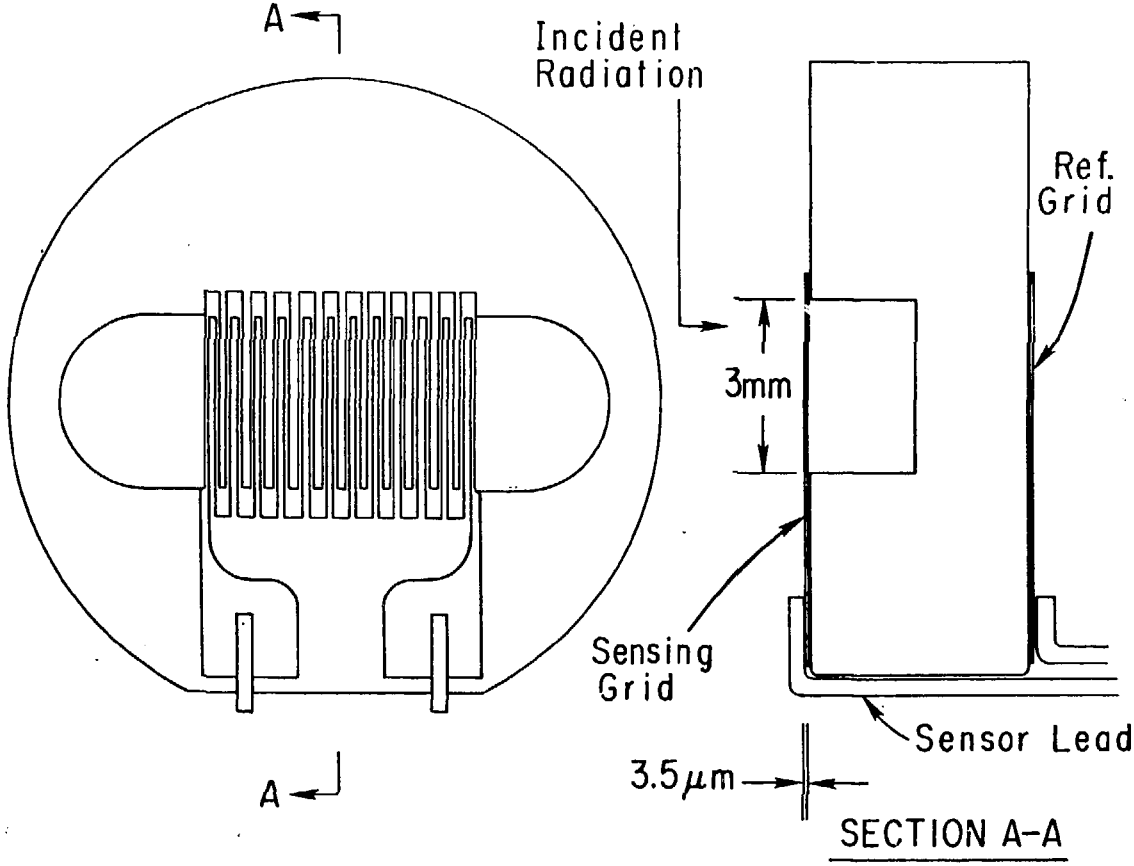
A
Incident
Radiation
Ref.
Grid
3mm
Sensing
Grid
Sensor Lead
A
3.5μm
SECTION A-A

Fig. 2

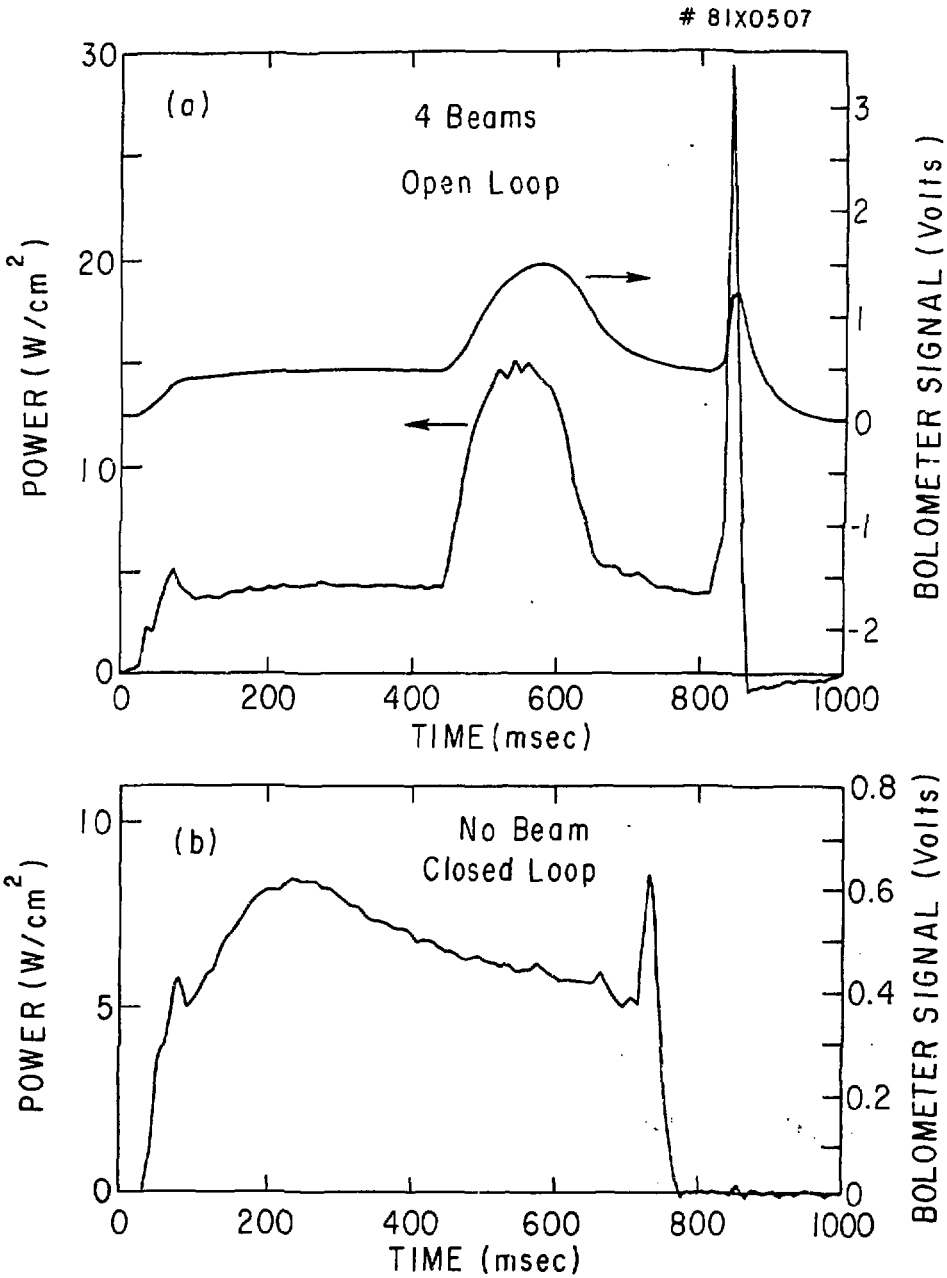
# 81X0507
(a)
4 Beams
Open Loop
POWER (W/cm²)
BOLOMETER SIGNAL (Volts)
TIME (msec)
(b)
No Beam
Closed Loop
POWER (W/cm²)
BOLOMETER SIGNAL (Volts)
TIME (msec)

Fig. 3

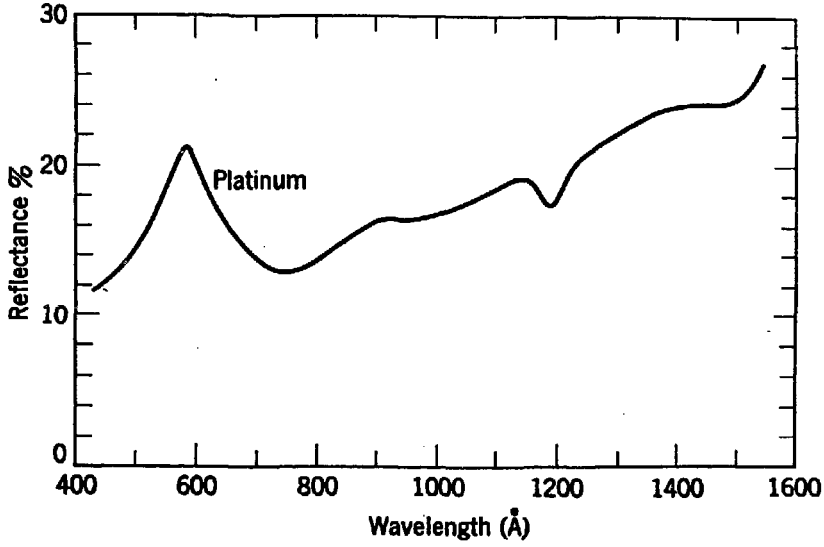
30
20
10
0
Reflectance %
Platinum
400
600
800
1000
1200
1400
1600
Wavelength (Å)

Fig. 4

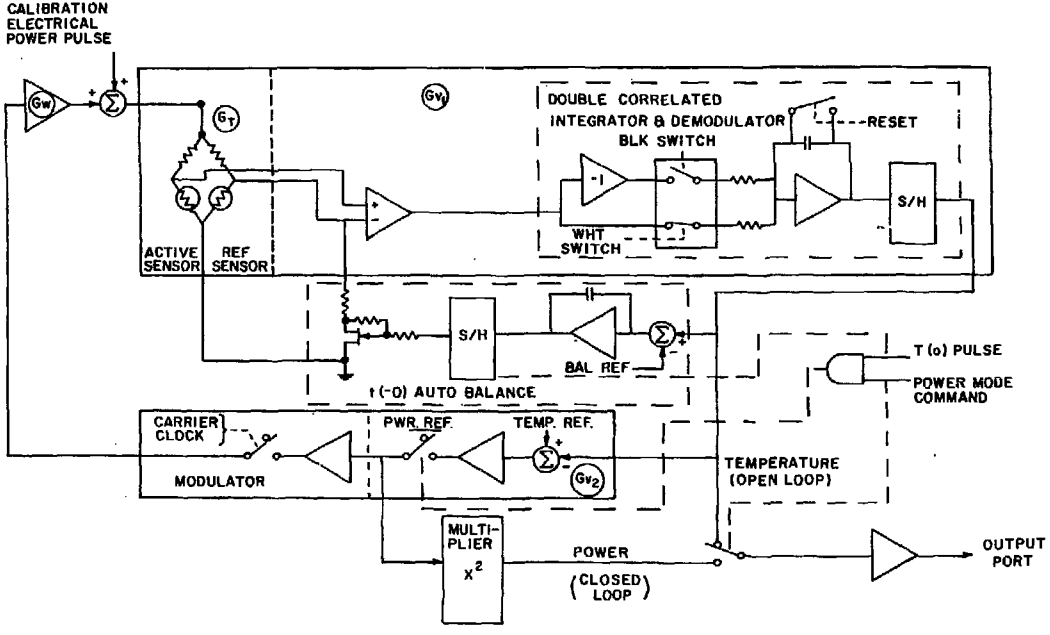


BLOCK DIAGRAM BOLOMETER ELECTRONICS

Fig. 5

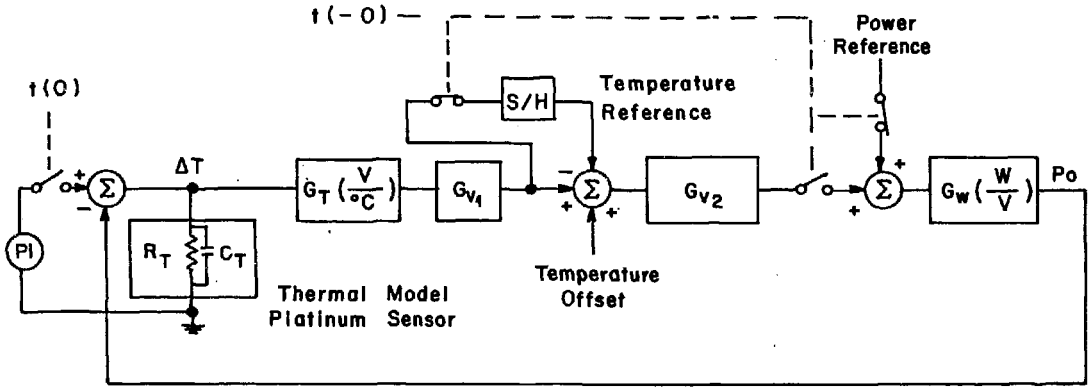


CONSTANT TEMPERATURE CONTROL SYSTEM

Fig. 6

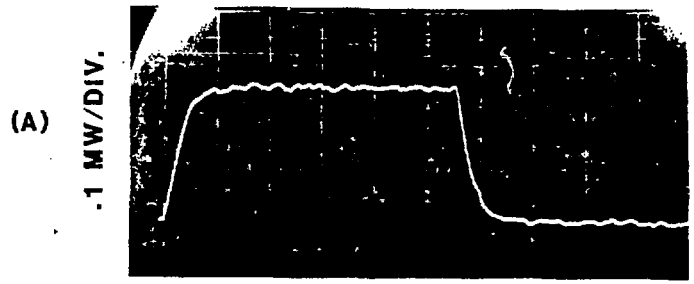


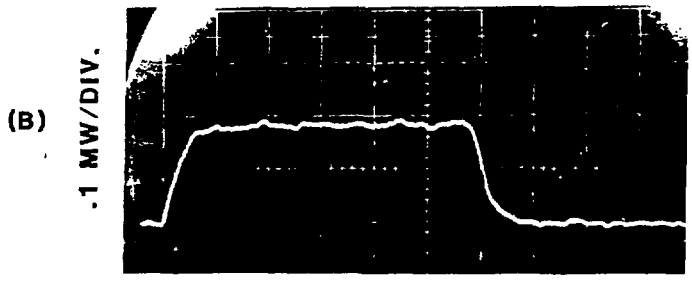


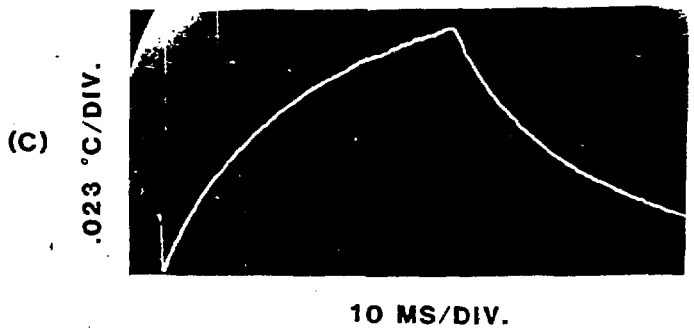


BOLOMETER RESPONSE TO AN INPUT POWER PULSE

Fig. 7

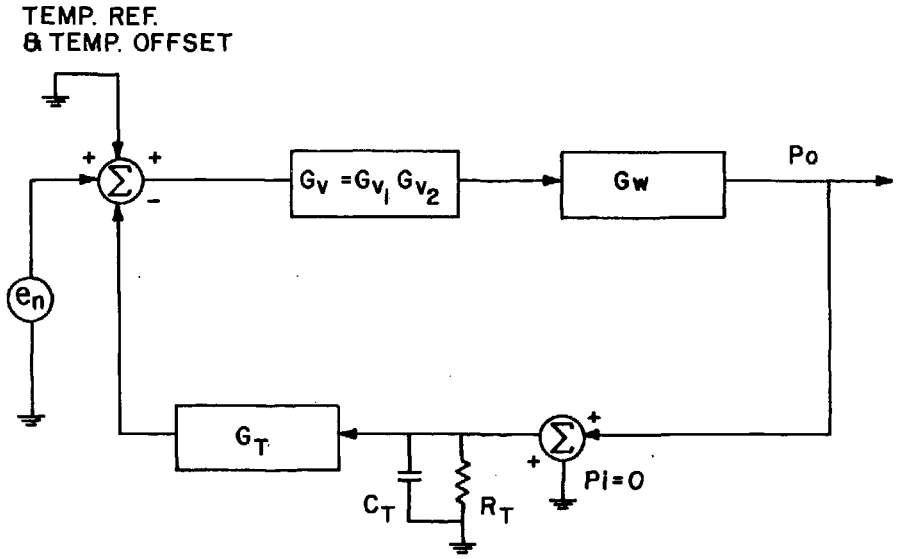


CLOSED LOOP NOISE MODEL

Fig. 8

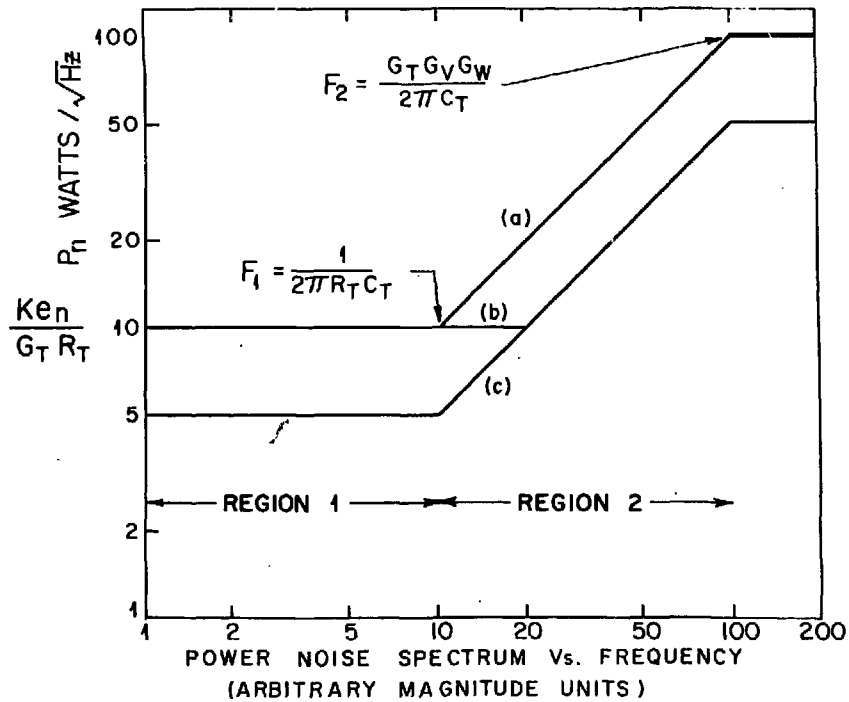
100
50
20
10
5
2
1
$\frac{Ke_n}{G_T R_T}$ $P_n$ WATTS / $\sqrt{Hz}$
$F_2 = \frac{G_T G_V G_W}{2\pi C_T}$
$F_1 = \frac{1}{2\pi R_T C_T}$
(a)
(b)
(c)
REGION 1
REGION 2
1
2
5
10
20
50
100
200
POWER NOISE SPECTRUM Vs. FREQUENCY
(ARBITRARY MAGNITUDE UNITS)

Fig. 9